Additive Manufacturing 111 (2025) 104974

Contents lists available at ScienceDirect

Additive Manufacturing

journal homepage: www.elsevier.com/locate/addma

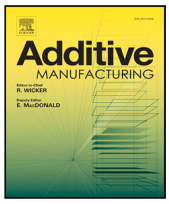

Research Paper

Enabling non-planar load oriented deposition of carbon fiber reinforced polymers by varying layer height

Johann Kipping *, Thorsten Schüppstuhl

Institute for Aircraft Production Technology, Hamburg University of Technology, Denickestr. 17, Hamburg 21073, Germany

ARTICLE INFO

Keywords:
Carbon fiber reinforced polymer
Layer height
Non-planar
Continuous fiber coextrusion
Fused filament fabrication

ABSTRACT

A common research goal for printing carbon fiber reinforced polymers (CFRP) using fused filament fabrication (FFF) has been the deposition along load paths to fully utilize the potential of the highly anisotropic material. Yet, the state-of-the-art solutions for load oriented non-planar slicing and path planning for neat polymers involve the dynamic variation of layer height. This variation is not possible in a single layer for the most commonly used process variant for printing CFRP, towpreg extrusion, because of the fixed ratio of matrix to fiber. This problem can be solved by printing interlayers which roughly double the layer count, introduce weak points, decrease the fiber volume fraction (FVF), and increase manufacturing time. Continuous fiber coextrusion (CFC) offers a possible solution to this problem, as the amount of polymer co-matrix can be controlled. This is possible because of the pre-impregnation of the fiber material, which allows active feed of both fiber and co-matrix. This study aims to investigate the possibility of using continuous fiber coextrusion to dynamically vary layer height during the printing process to enable the load oriented non-planar printing of CFRP. To this end, the process is described, a custom control scheme is mathematically derived, and an experimental plan is presented. The experiments include the printing of coupons to evaluate the minimum and maximum layer heights and the possibility to vary the layer height dynamically. A pipe and a bracket are printed to establish the applicability to manufacturing real-life parts. Micrographs are taken to assess the void content and fiber distribution. Surface roughness is evaluated with white light interferometry. To evaluate the impact of layer height variation on stiffness and strength, a mechanical investigation is performed involving tensile and compressive tests. In conclusion of this study, the possibility of dynamic layer height variation to continuous fiber coextrusion can be confirmed and its application for load oriented non-planar printing is enabled.

1. Introduction

Carbon fiber reinforced polymers (CFRP) are widely used in the construction of lightweight structures due to their excellent strength-to-weight ratio [1,2]. However, traditional manufacturing methods for CFRP are usually designed for shell-like structures and require the design and manufacturing of molds. This process can be costly and time-consuming [1]. CFRP printing using fused filament fabrication (FFF) offers a desirable alternative by allowing the production of complex geometries without the need for specialized molds in combination with the other advantages of additive manufacturing (AM) such as flexible and automated production, rapid prototyping and high degree of versatility [1,2].

Carbon fiber reinforced materials exhibit high degrees of anisotropy and show orthotropic material mechanical responses [3,4]. These properties account for the importance of fiber orientation and the printed mesostructure for parts with high strength, stiffness and toughness [4,5]. Continuous fiber composites exhibit far higher strength and stiffness than chopped fiber materials, making their potential for lightweight construction and combining the advantages of CFRP and FFF more attractive [6]. They are, however, more difficult to manufacture.

One major benefit of using FFF to print CFRP is the capability of load oriented placement of the fibers in order to account for the anisotropic properties of the material [7]. As material can only be deposited onto a printing surface or existing material with FFF, parts are built up in layers, which are also called slices. Structural optimization can be employed to compute the optimal material orientations given a specific loading scenario [8]. However, the optimal directions often exhibit out-of-plane characteristics. To follow the material orientations with the deposited bead, non-planar slices can be used with multi-axis manufacturing systems. The slices are then oriented as tangentially as possible to the optimal material orientations in order to achieve load orientation. To follow the optimal material orientations, one solution

* Corresponding author.
E-mail address: johann.kipping@tuhh.de (J. Kipping).

https://doi.org/10.1016/j.addma.2025.104974
Received 1 April 2025; Received in revised form 22 August 2025; Accepted 23 September 2025
Available online 6 October 2025
2214-8604/© 2025 The Author(s). Published by Elsevier B.V. This is an open access article under the CC BY license (http://creativecommons.org/licenses/by/4.0/).

that has already been demonstrated for neat polymer parts [9–11] is the dynamic variation of the layer height within each slice. For successful printing using this method, several process induced restrictions are required to be met, most prominently the range of allowed layer heights. Load oriented printing of CFRP in non-planar layers has been realized in promising publications without varying layer heights dynamically [12,13]. However, the process of using dual extrusion with a dedicated towpreg print head drastically increases the layer count and thus interlaminar surface area, which represent weak points in the printed part. Yavas et al. showed that, the addition of non-continuous fiber reinforced interlayers can reduce the interlaminar shear strength by up to 45% [14]. Neat polymer interlayers would also significantly reduce the possible fiber volume fraction (FVF) which is one of the major factors for stiffness and strength of parts. Additionally, it requires a switch of print heads for every layer containing CFRP, which increases the required manufacturing time.

Printing continuous CFRP with FFF presents an additional unique challenge: the brittle nature of the fibers means that the nozzle's travel distance must precisely match the length of the extruded fiber. If not, the result can be wavy deposition, fiber breakage, or incorrect fiber placement [15]. This requirement limits the use of towpreg extrusion systems for layer height variation, like those by Markforged, which cannot vary the ratio of polymer matrix to fiber. This inability limits the possible layer height range to the point where it is no longer feasible as a strategy for non-planar, load oriented printing of CFRP parts with layer height variation.

In-situ impregnation and coextrusion processes offer promising alternatives, although in-situ impregnation has struggled to produce high-quality parts due to insufficient impregnation times and inadequate fiber wetting [16]. It is believed to have limited capability of dynamic layer height variation due to the inability to actively feed the dry fibers. Anisoprint, a prominent company in the field of FFF with CFRP, uses a coextrusion process that combines pre-impregnated fiber with a "co-matrix" during deposition [17]. Their process is advantageous because the pre-impregnated fiber material includes a "special polymer blend" with both thermoplastic and thermoset properties, enabling active advancement of both the co-matrix and fiber material.

The coextrusion process allows for dynamic adjustment of the amount of co-matrix by varying the relative material feed. This capability, crucial for load oriented and non-planar printing with dynamic layer height variation, has not yet been scientifically explored. This study examines how this feature can be used to vary layer height and tests the applicability to real-world parts. Additionally, it investigates how varying the fiber volume fraction affects the composite material properties and performance.

1.1. Prior work

This section aims at describing the existing literature in the fields relevant to this work. First, the continuous fiber coextrusion (CFC) process and publications regarding layer height and its variation are presented, followed by experimental investigations of general continuous CFRP materials for the FFF process. Then, layer height in the classical FFF process is discussed, concluding with the two thematically closest publications to this study. Finally, after a short description of the state of the art regarding print head design and extrusion control the research questions, aims, and structure of this work are presented.

The CFC process was first scientifically presented and published in [17] under the name of "Bi-Matrix Composite 3-D Printing Technology". The publication contains details on the idea, working principle and materials used at time of publication. It was noted, that higher fiber volume fractions can be achieved with the towpreg extrusion method, where a thermoplastic matrix is used, but the gained flexibility of the CFC process is said to be worth the loss in FVF. The patent for this process can be found in [18]. In [19] the Anisoprint print head is mounted to an articulated 6-axis robot arm and is used to print curved pipes. The publication does not clearly state if varying layer height was used to curve the pipe, it rather suggests that serpentine movements were used to create the curvature.

Table 1
Layer height ranges and optima found in the literature for the Anisoprint CCF Material, all values in millimeters.

Source	Range	Method	Optima
[20]	[0.24, 0.34]	Short beam shear	0.34
[22]	[0.32]	Tensile and flexural	0.32
[23]	[0.36]	Tensile and numerical	0.36
[24]	[0.2, 0.3]	Tensile and flexural	0.2/0.3
[25]	[0.38, 0.58, 0.78, 0.98]	Flexural	0.38
[26]	[0.4]	Tensile	0.4
[27]	[0.36]	Flexural	0.36
[28]	[0.2, 0.3]	Tensile	0.2

Investigating the existing literature, there is no clear consensus on what the minimum or maximum layer height for FFF with CFRP using coextrusion or even other methods and materials are. Several sources state different values for the layer height. The lowest is stated to be 0.06 mm in [17], in [20] a layer height of 0.24 is used and in the official documentation for Anisoprints slicing software Aura [21] 0.36 mm is stated as the minimum layer height for the fiber layers corresponding to the diameter of the fiber filament. This uncertainty underscores the need for a structured investigation of layer height as a printing parameter in the coextrusion process. Many studies that include mechanical tests found in the literature do not give any indication on layer height used in the experiments. The relevant studies that evaluate the mechanical properties, do give indication on the layer thickness and use the Anisoprint continuous carbon fiber (CCF) Material can be seen in Table 1. The identified optimal layer height is given in the right column.

The studies collected in Table 1 and studies on mechanical investigation of CFRP parts manufactured with FFF not using the Anisoprint material are presented in the following.

Almeida et al. [20] investigate printing parameters by testing interlaminar behavior within short beams. The best parameter combination is determined as a layer thickness of 0.34 mm, extruder temperature of 220°C, and print speed of 5 mm/s. With 0.34 mm being the highest tested layer height, behavior above the stated optimum layer thickness is not examined. Andreozzi et al. [22] explore the effects of moisture on tensile and flexural properties, revealing that a decrease in moisture content enhances these properties. Furthermore, void content was found to increase moisture absorption rates. To counteract these effects, coatings are suggested as a viable solution to minimize moisture uptake. Ding et al. [29] investigate the interaction of layer height and path spacing using various FRP filaments, although without active material delivery. Their research indicates that reducing layer height improves bending strength, suggesting an optimal layer height range of 30%–40% of the fiber diameter for thermoplastically impregnated fibers. Due to the thermoplastic matrix, the results are minimally applicable to this work. Similarly, Dou et al. [30] investigate, among other things, the influence of layer height for a 1k carbon fiber material and PLA as matrix. They state that layer height has an even greater impact in FFF with CFRP than classical materials, as it highly influences the FVF. They observe a clear increase of tensile stiffness and strength with decreasing layer height. Extrusion width is observed to have a similar impact, with lower extrusion width increasing the fiber volume fraction and thus stiffness and strength. Printing temperature and speed are observed to play a minor role, with higher temperature and lower speed achieving the best results. The main weakness is determined to be fiber pull out. The influence of infill parameters is further examined by Gao et al. [23], who studied the effects of infill density and carbon fiber-reinforced perimeters on mechanical properties, revealing critical insights into fracture behavior. Kasmi et al. [31] report on infill orientation effects using Anisoprint filaments. They state 0.2 mm as

layer height and 50 mm/s as printing speed, which are improbable to have been applied to the fiber layers, as 50 mm/s far exceeds the maximum of 10 mm/s given as maximum printing speed by Anisoprint. Material choice and printing strategies have significant implications, as evidenced by Kong et al. [24], who found that bi-matrix coextrusion enhances structural strength when printing complex geometries with cavities. Effects of fiber bundle size where shown to not have significant impact on tensile strength by Vatandas et al. in [32]. Li et al. [33] used Markforged material and printer to do a full mechanical characterization with tensile, compressive, bending and Charpy impact tests. All specimens were analyzed for their fracture behavior, stiffness, and strength. The compressive specimens were only tested with a fiber orientation transverse to the loading direction. Liu et al. [25] performed thorough investigation into the print parameter's effect on the resulting flexural strength with Anisoprint PETG and CF materials. The main findings are as follows: the CFC bi-matrix approach seems to solve the issue of poor impregnation, for good quality, print speed should be kept below 7.5 mm/s, larger hatch-spacing or path distance increases porosity, layer thickness has a great impact on the flexural stiffness and strength due to increased FVF. They identified the lowest tested layer height as the optimum of the parameter range, so the effect of lower layer heights than 0.38 mm was not examined. Thus, the possibility that lower layer heights would perform even better cannot be excluded. Furthermore, only flexural and not axial strength and stiffness were examined.

Following the previous publication Liu et al. [34] further analyze the influence of process parameters on two interface behaviors and mechanical characteristics of the composites made with the Anisoprint PETG and CF materials via a combination of experimental methodologies and computational investigations. Through 3-point bending tests, the flexural properties under different processing parameters are provided, and the bending failure modes are assessed by combining meso- and microstructural characterization. The layer height was held at a constant 0.36 mm for all investigations in this study. Parmiggiani et al. [35] investigate the influence of fiber orientation using the Markforged material. This study found that mixed orientations can be a promising solution to multiaxial stress states. Rimasauskas et al. [36] studied the influence of layer height and line width on stiffness and strength. They also found a reduction in both to be beneficial to stiffness and strength, although they only tested 0.3 mm and 0.4 mm as layer heights. T300-1000 carbon fiber made by Toray was used in conjunction with PLA.

The fracture behavior of short fiber CF-PEEK composites has also be shown to be influenced by layer height. A larger layer height was shown to impact fracture energy for crack growth due to larger defects in taller layers [37]. Furthermore, interlaminar shear strength of these composites has been shown to also be negatively impacted by larger layer heights by up to two to three times [38].

Savandaiah et al. [27] introduces a post-processing technique where rapid consolidation was used to reduce void content.

In the general research on FFF printing, there exist several publications that investigate the effect of layer height, of which the most relevant to this work are presented in the following. Butt et al. [39] tested the influence of line width and layer height on measuring mass, dimensional accuracy, surface roughness, hardness, and fracture loads for 4 neat polymer materials. They state that with larger layer height, the microstructure indicates larger voids and cracks, leading to reduced strength. Fischer et al. [40] investigate the influence of nozzle diameter and layer height on part quality. The main findings are that yield strength increases for larger nozzle size but smaller layer height. They obtained the densest mesostructure, the lowest surface roughness and the best mechanical properties for the smallest nozzle diameter and smallest layer height. Additionally to reduced voids for lower layer heights they state that re-entanglement, interdiffusion of the polymer, total contact surface area and the number of welds have an impact on strength but identify the nozzle diameter and not layer height as the prominent parameter for these effects. Garzon-Hernandez et al. [41] present a modeling methodology to investigate the sintering effect of neighboring deposited material beads. Higher elastic modulus and maximum stress are observed for lower layer heights and longitudinal raster orientation, although a higher number of layers also negatively impacted the results. They also found a decrease in void density with the sintering effect. Pelzer and Hopmann [42] vary the layer height to create non-planar layers without a 5-axis machine. The conclusion from these publications can clearly be denoted as lower layer height being desirable for improved strength and part quality. This is mostly believed to be caused by a denser mesostructure of the part for lower layer heights.

The two most thematically close studies to this work, as they have the main goal of investigating layer height variation, are the following. Kumekawa et al. [43] varied the thickness of an extruded towpreg without changing FVF, by only changing the nozzles distance. This was found to result in bad compaction, that leads to a limited viable range between 0.09 mm and 0.17 mm. A simultaneous optimization of fiber path and thickness is applied and experimentally investigated.

Zhang et al. [44] present a method for line width prediction of printed CFRP using the coextrusion process based on the principle of material conservation. Bead cross-section was analyzed in relation to the layer thickness, the fiber–resin relative extrusion rate and the nozzle tip geometry. The effects of heating block temperature, overlap rate, FVF, fiber bundle type, and printing speed on the flexural properties of 3D printed CCF/PP composites were also analyzed. Slower print speeds and higher fiber content were clearly identified as beneficial to tensile strength.

The print head used in this work is methodologically derived, designed, constructed and tested in [45]. A cut view of this print head design especially developed for the CFC process and avoiding collisions by having a high clearance angle can be seen in Fig. 1 taken from [45]. The publication also includes an evaluation of previous work. Thus, in the next section only a small overview on the state of the art is given, while excluding research regarding towpreg extrusion methods and focusing on continuous fiber coextrusion.

Cai and Chen provide a review on printheads for FFF of CFRP [46]. They state that the present challenges arise mainly from the coordination of the equipment, process parameters and extrusion methods. It is furthermore identified, that the print heads have a great impact on the process stability and quality of parts as they have to ensure precise and consistent deposition of the composite. Another important stated factor is the nozzle geometry as it is central for successful deposition and clogging of the nozzle has been a regular issue. This is why special rounded off nozzle have been developed, which are often also made of harder materials to prevent wear. The difference of the nozzle geometry compared to classical FFF is compared in a later section of this work.

The print head developed by Anisoprint that is the groundwork for the print head used in this work is presented in [17] and its patent [47]. The printing system used in this work is also methodically developed and described in prior work [48].

As was shown, the mechanical method of delivering the material has a high impact on part quality. Controlling these mechanical devices is another topic with high impact. As the volume of extruded material is difficult to measure, feed-forward approaches are being used in FFF. In [49], a linear and nonlinear extrusion controller are devised, and the control scheme is described in detail. Both methods were successful in reducing defects resulting from changes in the nozzle's movement speed. As an application, variable width extrusion was mentioned where the benefit would be large. In a subsequent publication, Wu et al. additionally investigated the control of filament advancement and retraction [50].

Concluding the discussion of prior works, the aims of this work are presented in the form of the following research questions:

1. How can the continuous fiber coextrusion be applied to non-planar multi-axis printing?

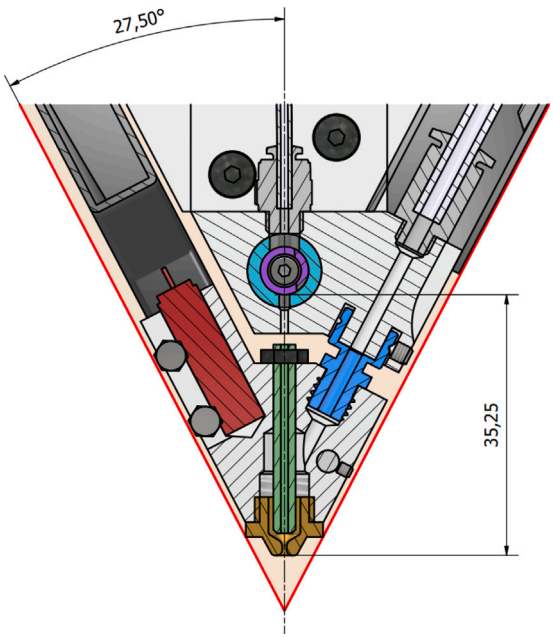

Fig. 1. Cross-sectional view of the print head used in this work taken from [45]. The angle denotes the collision-free tool angle and the length denotes the minimum fiber cut length. Green: fiber tube, blue: heat break, red: heating element, teal: cutting sleeve, purple: cutting blade. The polymer co-matrix filament is added to the mixing chamber through the heat break marked in blue and the fiber material is fed through the fiber tube marked in green. Mixing of the fiber and co-matrix material is located at the nozzle orifice. (For interpretation of the references to color in this figure legend, the reader is referred to the web version of this article.)

2. What is the minimum and maximum layer height of the continuous fiber coextrusion process?
3. Is this layer height variation possible dynamically?
4. Can this be applied to manufacture parts?
5. How do stiffness, strength vary with fiber orientation, fiber volume fraction and layer height?
6. What quality regarding voids and surface roughness can be achieved?

The Section 2.2 aims at answering research question 1 with questions 2–6 being answered by experimental works described in Sections 2.3 and 2.4.

2. Materials and methods

2.1. Materials

For all tests in this work, the materials sold by Anisoprint specifically for the use in their coextrusion system are used. Due to the active material feed of the fiber, a thermoplastically impregnated material would immediately clog the nozzle upon exceeding its glass transition temperature. This is why Anisoprint uses their ”special polymer blend” to impregnate the 1.5-K tow, which seems to exhibit both thermoplastic and thermoset properties.

The CCF material sourced from Anisoprint is stated to have an elastic modulus of 149 GPa, a tensile strength of 2206 MPa and a FVF of 60% as reported in the technical datasheet. It consists of a tow of 1.5-K carbon fibers.

As co-matrix, the recommended PETG material supplied by Anisoprint for the CFC process was used. For the water-soluble support, PrimaSelect™ PVA+ in natural color was used.

2.2. Process and extrusion control

As described in the motivation in Section 1, slicing solutions exist that can follow the out-of-plane optimal material orientations [9–11]. However, they require the variation of layer height in order to construct the load oriented slices. The fiber material can only be deposited at the same velocity that the printhead is moving at, otherwise the fiber material breaks or is deposited in an irregular, wavy pattern. Thus, the height of the deposited bead has to be varied through the ratio of polymer material added during the deposition process. As active material feed is required for feeding the material after cutting the fiber in this configuration, the fiber material is pre-impregnated making it stiff enough for feeding. This defines the use of continuous fiber coextrusion. By feeding both materials actively, the fiber can be controlled to feed corresponding to the print head speed and the amount of thermoplastic co-matrix can be controlled to create the set layer thickness. The mathematical derivation of the control scheme developed to this end is described in a later part of this section. The materials mix in the mixing chamber of the printhead, seen in Fig. 1. The CCF material is fed through a tube until just before the nozzle orifice in order to keep the fiber straight and to avoid excessive backflow of the co-matrix.

A requirement put on the process by the non-planar multi-axis movement is collision avoidance. The print head is specially designed with a large clearance angle in order to prevent collisions with the print bed or already deposited material. The nozzle geometry has rounded features at the orifice to compact the deposited bead and to avoid breaking the fiber. This assembly is put on a multi-axis printing system that guides the print head along the planned path while controlling the extrusion process.

As stated above, extrusion control is essential for accurate deposition and enabling dynamic layer height variation. The comparatively fast motion system has to be synchronized with the comparatively slow extrusion system. The dynamics of motion control are handled by the robot controller, which can be considered as sufficiently linear, especially for slow movement [49]. The extrusion system on the other hand can exhibit nonlinear dynamics, but feedback control for the extrusion system is difficult to implement directly. It is often done by indirectly inferring the extrusion rate from the extruder feed or other indirect measurements. A classical approach to simplify the problem is linear feed-forward control with a static gain pretuned by the user. This method is chosen in this work as the movement speed is low, but advanced control systems can be applied in the future if deemed necessary. No significant transient effects are expected for any experiments done in this work, as 5 mm/s is the chosen as the movement speed. As this classical method, which is well described in [49], is chosen for the co-matrix feed, this work only combines the process of CFC with the classical methods to enable dynamic layer height variation. The detailed description and mathematical derivation in this chapter serves the purpose of clarity and completeness as its functionality has a significant impact on the actually printed layer heights and mesostructure.

The extrusion control is implemented on the robot controller’s PLC. All dynamics are assumed to be linear, an assumption guided by the slow movement speed. This method can and should be improved further, yet no defects like over- or underextrusion could be observed, even in regions of dynamic movement and direction changes. Furthermore, the motion control is fully handled by the robot, with the current speed v_{rob} resulting from internal computations of the controller.

To implement the feed-forward control for the extruders, their angular motor velocity ω has to be determined. This is proportional to the material advancement velocity out of the nozzle $v = \omega/k$, with k being a measurable factor dependent on the extruder gearing. In this section, the subscript f and m are used to distinguish between fiber and co-matrix.

As mentioned in Section 1, the length of deposited fiber has to be equal to the traveled distance leading to $v_f = v_{rob}$ and thus $\omega_f = k_f v_{rob}$

for the fiber extruder, with v_{rob} being the robot's movement speed. In order to compute v_m and thus $\omega_m = k_m v_m$ for the co-matrix extruder, material conservation is assumed where the volumetric extrusion rate of the deposited bead Q_d and the volumetric material feed rate at the extruder Q_e are assumed to be equal. With the cross-sectional areas of the deposited bead A_d, filament material A_m and fiber, A_f the following equation can be established for the co-matrix extruder:

$$Q_d = A_d v_{rob} = A_m v_m + A_f v_f = Q_e \tag{1}$$

The filament material diameter d_m and fiber diameter d_f are used to compute $A_m = \pi(d_m/2)^2$ and $A_f = \pi(d_f/2)^2$ respectively. The robot velocity v_{rob} is directly obtained from the robot controller during the printing process. The factor k can be determined by turning the extruder motor a full turn and measuring the length of advanced material directly out of the extruder, before the nozzle. The extruded length is the inverse of k.

The final parameter to compute ω_m is the desired cross-sectional area of the deposited bead A_d. It is given by $A_d = hw$ with height h and path spacing w establishing the dimensions of the bead. The height h is set with every movement instruction in order to be able to dynamically vary it. The path spacing w is set to a constant value in this work, although it can be varied in the future to decrease voids in areas of inconsistent line spacing. Rearranging (1) yields the method for computing the co-matrix extruder's rotational velocity, with the only dynamically varying parameters being the robot speed v_{rob} and the height h as

$$\omega_m = k_m v_m = k_m \alpha \frac{A_d v_{rob} - A_f v_f}{A_m} = k_m \alpha v_{rob} \frac{hw - A_f}{A_m}. \tag{2}$$

The additional parameter α is set as a calibration factor to enable the user to fine trim in order to avoid over- and underextrusion. This is necessary due to the geometry of the deposited bead not being a rectangle but rather having overlap and merging with neighboring beads and the fact that the factor k is calibrated by the user, which is error-prone.

The computations described above are also valid for the neat polymer extruder when setting $A_f = 0$. One full motor turn results in roughly 8 mm of extruded filament thus $k_p = 0.125\ 360°/mm$ for the neat polymer extruders, 23 mm for the co-matrix extruder thus $k_m \approx 0.043\ 360°/mm$ and 38.5 mm for the fiber extruder thus $k_f \approx 0.026360°/mm$, resulting from the specific models built into the printing machine used in this work [48]. Small errors in this measurement are easily compensated for by the calibration through α.

In Fig. 2, the recorded extrusion control parameters can be seen during the printing process of printing the coupon for testing dynamic layer height variation described in Section 2.4. In the top, the robot velocity v_{rob} is plotted. The direction changes at the end of the rectangular coupon can be seen as smaller dips in the graph, the larger dips correspond to layer changes. The fiber feed rate corresponds exactly to this speed, while the co-matrix is affected by the set layer height seen at the bottom of the plot and the robot speed. The layer height varies up and down linearly as the printed coupon has a thicker section and a thinner section at the ends.

2.3. Targets and parameters

This section aims to describe the experimental target values guided by the research questions and the relevant process specific parameters. In the first part the selected target values are motivated and explained, in the second part all identified parameters with their respective preset values or value ranges are presented.

The following targets have been chosen in order to answer the research questions 2–6:

- Layer height range
- Dynamic layer height variability
- Process applicability
- Stiffness and strength
- Quality (Voids and fiber distribution)

The process of additively manufacturing CFRP parts with FFF is analyzed regarding relevant process parameters, while taking the research goals into consideration. The parameters are grouped by temperature, geometry, extrusion, speed and material, which will be presented in the following. The listing is not exhaustive but includes the parameters relevant to this work.

Hotend and bed temperature have great influence on a material's extrusion and adhesion properties. For the Anisoprint CCF material and co-matrix combination, the recommended temperature of 240 °C was set for all experiments, which has also been identified as suitable in [25]. Active cooling of the extruded material has been identified not to be necessary with the current setup, as no overhangs are printed and heat input into the printed part is minimal due to low extrusion rate and manufacturing speed. This should be the object of further investigations in future works. Bed temperature was set at 70 °C for all experiments.

Regarding geometrical parameters, the nozzles distance to the printing surface or existing material is one of the most central parameters in this study, as it dictates the resulting layer height in the nominal case. This parameter is varied across the experiments, which are described in Section 2.4. To guarantee sufficient precision for the first layer, the printing system is calibrated by adjusting the robot's base coordinate system. The key factor for the precision of subsequent layers is the robot's accuracy, which is stated to be 0.02 mm by the manufacturer. Another geometrical parameter is the fiber orientation. This is directly determined by the path planning and resulting movement of the printing unit. In this work, fiber direction is only controlled in the experiments on stiffness and strength described in Section 2.4. For all other experiments, this parameter is kept at fully parallel lines with constant path spacing. The path spacing is chosen to be 0.65 mm, which is the standard value used by Anisoprint and has also been identified as optimal regarding voids in [25].

The extrusion control system was described in Section 2.2. As mentioned, the calibration factor α is a parameter set to be calibrated by comparing the desired and measured extrusion width, which is done in preliminary tests. For all experiments unless otherwise stated, this calibration factor was set to 1.02. Fiber feed rate is always set to be exactly corresponding to the traveled distance to prevent fiber breakage, clogging or wavy deposition. This is also achieved by accurate control with a PLC and calibration through setting the extrusion factors k_p, k_m and k_f. Retraction is not necessary in the set of experiments and is thus not included. As stated above, the tests furthermore do not include any overhangs.

Manufacturing times are most prominently affected by the printing speed. The manufacturer's recommendation for printing the CF material is the range from 1–10 mm/s. As manufacturing time is not the focus of this work, and it was identified as a safe value for the PETG to have enough time to melt in [25], 5 mm/s is chosen for every experiment.

2.4. Experiments and testing plan

In this section, the experimental procedures are described. For each of the research questions 2–5 established in Section 1, a subsection and corresponding experimental plan is presented. Research question 6 is individually addressed in the subsections of this section. Prior to the experiments, preliminary tests have been conducted in order to estimate material behavior and calibrate the printing machine's extrusion factors and coordinate systems. As stated in the introduction, the print head and printing system used in this work are methodically derived and presented in [45,48].

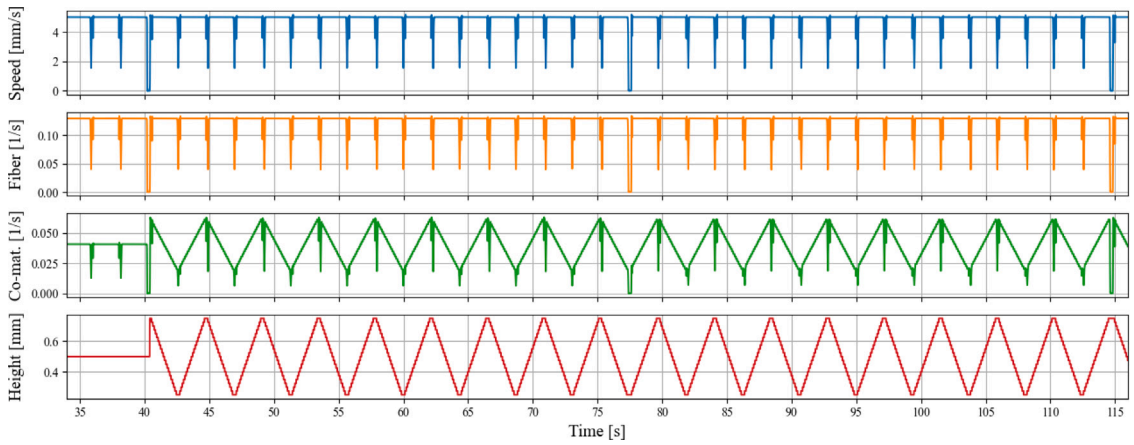

Fig. 2. Extrusion control parameters during printing process of dynamic layer height test coupon from Section 2.4. From top to bottom: robot movement speed, fiber extrusion velocity, co-matrix extrusion velocity, commanded layer height value. The robot speed can be seen to proportionally influence fiber extrusion and co-matrix extrusion. The co-matrix extrusion is also dynamically adapted to reflect the target layer height, which enables the dynamic layer height variation.

2.4.1. Layer height range

The defining factor for the load oriented printing approach motivated in Section 1 is the capability of varying the layer height in order to build up slices matching the optimal material orientations. It has been identified as necessary in [9–11] to ensure $2h_{min} \leq h_{max}$ in order for the approach to be suitable, with h_{min} being the minimum and h_{max} the maximum allowed layer height. Due to the importance of this requirement, the first experimental tests are conducted to find the permissible range of layer heights with the process and equipment used in this work. This range is mostly thought to be influenced by the fiber material's diameter on the lower limit and the layer adhesion, void formation, undefined extrusion and heat transfer on the upper limit. The lower limit is regarded to be a more fixed limitation, as the fiber material has a known and absolute diameter. The CCF material's cross-section area is $\pi(d_f/2)^2 = 0.0962$ mm^2 and thus the absolute minimum layer height where the deposited material bead only consists of the CCF material would be $h_{min} = 0.092\ mm^2/0.65\ mm = 0.148$ mm, for a path spacing of 0.65 mm. This layer height is impossible to manufacture, as the presence of only matrix with thermoset properties will prevent the necessary fusing of existing and deposited material. Furthermore, for layer heights below the CCF material's diameter, a change of cross-section is required. It is not clear how this flattening affects the pre-impregnated CCF material. As the matrix is not thermoplastic, it is not expected to be easily malleable, which might lead to the formation of voids and severe cracking upon deformation.

Path spacing, which has been chosen to as 0.65 mm also has a high impact on the deposited bead's cross-sectional shape. It is conventionally assumed that the layer height should be a fraction of the path spacing as the extrusion process relies on flattening the deposited bead in order to reach a defined geometry, as can be seen in Fig. 3(a) for a nozzle used in classical neat polymer FFF. Due to the required nozzle shape for printing CFRP, the bead is only pressed down in the nozzles moving direction, as can be seen in Fig. 3(b). For layer heights exceeding the path spacing of 0.65 mm, the cross-sectional shape of the bead is undefined, as it is not pressed down and flattened by the nozzle. Due to the unknown upper limit, the effect of this missing flattening is to be experimentally evaluated regarding producible quality when the layer height exceeds path spacing.

As mentioned in Section 1.1, there is no clear consensus on what the limits on layer height are, so the range is kept very open. With the reasoning described above, the range of layer heights to be tested is set as $h \in [0.2, 0.25, 0.3, 0.35, 0.4, 0.6, 0.7, 0.8, 0.9]$ in millimeters.

The specimens manufactured in these initial tests are coupons consisting of 10 layers stacked on top of each other with the same parallel line paths. Each layer consists of 16 lines with 0.65 mm path spacing and 20 mm in length, which results in the dimensions $20 \times 10.4\text{x}H$ mm with $H = 10h$ being the height of the specimen corresponding to the set layer height.

After identifying a printable range, micrographs are to be done to identify possible voids. Furthermore, the fiber content is experimentally determined by mass. The fiber mass fraction can be calculated from the difference in mass of specimens before and after extraction of the resin by sulfuric acid digestion, adhering to the DIN EN 2564. The fiber content is reported as a percentage of the initial mass. This method is highly precise but does not take voids into account. This was done to ensure high enough accuracy of the resulting data. To assess void content through cross-sectional analysis a much higher sample size would be desirable as the void content is expected to vary inside the probe.

2.4.2. Dynamic layer height variability

In order for the constituting layer to orient along the optimal material orientations the layer height not only has to be varied between h_{min} and h_{max} statically, it also has to be achieved dynamically. To investigate the extent to which the CFC process is able to achieve this, the tests described in this section are constructed similarly to the previous test. The previously determined maximum layer height is set at one end of a coupon and the determined minimum layer height at the other end. By stacking layers in this way, a trapezoidal shape is created in the X-Z plane. To investigate the extent of dynamical variation capability, specimens of different coupon lengths are manufactured. Shorter lengths correspond to faster variation of layer height. Taking the nozzle's clearance angle into account, the minimum distance to vary between maximum and minimum layer height was chosen to be 10 mm. A length of 30 mm was chosen to be regarded as a viable maximum in this test run. With this reasoning, the range of parameter l corresponding to the length of the coupon is set as $l \in [30, 20, 10]$ in millimeters for the experiment.

2.4.3. Process applicability

With the process parameters examined, the developed system is to be tested in the application of manufacturing parts. The part geometries are chosen to test for the ability to vary layer height and produce part geometries and inner structure that are not possible to create by the existing manufacturing processes for printing CFRP parts with FFF. The parts furthermore require non-planar deposition.

The first part is a simple V-bracket, which tapers on both sides. The slices and paths for this part can be seen in Fig. 4(a). When manufacturing this part with planar FFF, it would exhibit a high degree of stair-stepping and the optimal part orientation would not be easy to

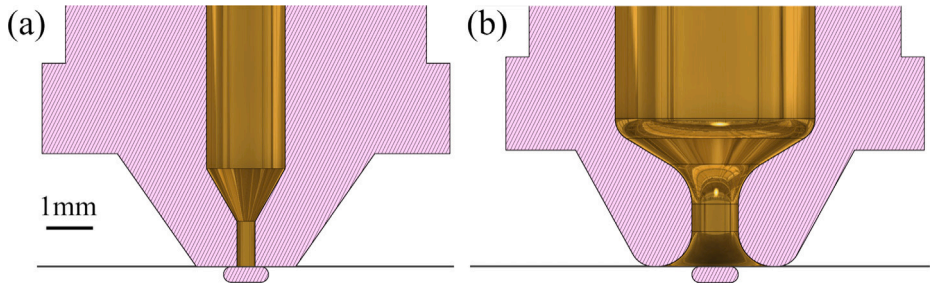

Fig. 3. Cross-section of nozzle geometries for nozzles used in: (a) classical fused filament fabrication with neat polymers with 0.4 mm bore diameter, (b) fused filament fabrication of carbon fiber reinforced polymers with the continuous fiber coextrusion process used in this work with 1 mm bore diameter. The rounded nozzle orifice exit is employed to prevent fiber breakage. The larger internal cavity in the CFC nozzle is necessary as the fiber material and polymer co-matrix are mixed inside this cavity and the fiber tube has to fit into it.

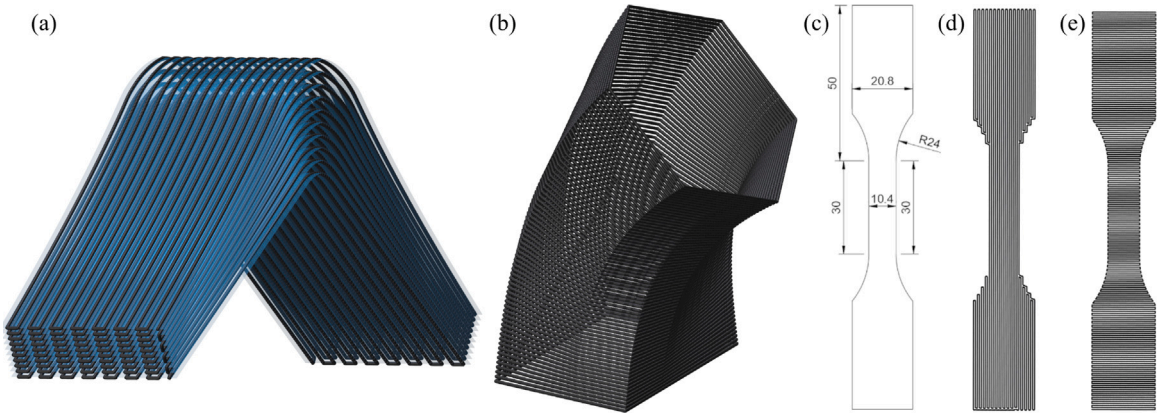

Fig. 4. Parts for the verification of the process applicability: (**a**) V-Bracket with dimensions 10 mm x 43.5 mm x 17.3 mm and (**b**) Tube structure to demonstrate the variation of layer thickness and reduction of necessary layers and non-planar deposition with dimensions 42 mm x 52.5 mm x 76.7 mm. (c) Dimensions of dogbone specimen used for investigation of mechanical properties. (d) Paths in X-direction for the dogbone specimen. (e) Paths in Y-direction for the dogbone specimen.

determine as only one side can be manufactured to align with the slices and thus the fiber direction. It would furthermore consist of a high number of layers, increasing the effect of the weakest interlayer adhesion. With a multi-axis machine and non-planar deposition, the layers are able to conform to the shape of the bottom face of the bracket, decreasing the number of layers. However, without the capability of varying layer height the tapers at both ends would still result in a stair-step effect and an increased layer count, even if non-planar printing is used. If this part geometry can successfully be manufactured by the method presented in this work, it would demonstrate the applicability of this process to volumetric parts and furthermore show the possibility to decrease layer count and the stair-step effect. In order to be able to print the structure, supporting material has to be used to construct a base on which the first part layer can be placed. This is chosen to be PVA in the experiments to increase the ease of removal. The paths for the V-bracket are created with a custom script written in python.

To apply the process to a part that is not practically manufacturable without layer height variation and thus further demonstrate the capability of this process, a tube-like structure is to be printed, which can be seen in Fig. 4(b). The pipe features a bend and constantly changing cross-section. This requires the layer height to be dynamically adapted to increase the height of each layer on the outer side of the bend and decrease it on the inner side. The printing paths for this geometry are created with a self-developed custom slicer for tube-structures presented in [51].

2.4.4. Stiffness and strength

To investigate how stiffness and strength vary with fiber orientation and layer height and thus answer research question 5, tensile and compressive tests are conducted, which will be described in this section.

For the tensile tests, a dogbone geometry inspired by DIN EN ISO 527 (Appendix A) is chosen. To be in the permissible thickness range with varying layer height, every specimen is chosen to consist of 3 layers. This choice is furthermore motivated by the inability to construct dogbones of identical height directly through printing due to the discrete nature of the layer height. Therefore, the layer number is kept the same over the tests, with the dogbone thickness varying. As the amount of fiber is identical with this approach for all specimens, the effect on stiffness and strength of varying the layer height is expected to be only influenced by the additional co-matrix material or any effects due to layer height variation. As manufacturing the dogbones in a standing orientation to investigate the interlayer adhesion is impractical, only the intra-layer effects of fiber orientation along and across the fiber direction are chosen. Furthermore, the interlayer adhesion is expected to be weaker than the intra-layer adhesion and the difference of the fiber taking the load to the co-matrix taking the load is expected to be the prominent factor. The chosen values for determining the effect of layer height on the tensile strength are $h \in [0.3, 0.5, 0.7]$ in millimeters with 6 specimens manufactured for each fiber orientation, where X denotes axial loading along the fibers and Y denotes loading orthogonal to the fiber direction. This parameter combination results in 36 specimens for the tensile tests. A ZwickRoell Z010 universal testing machine is used for the tests, which can be seen with the mounted specimen in Fig. 5(a).

As the dogbone widths according to DIN EN ISO 527 (Appendix A) are not a multiple of the path spacing 0.65 mm, the geometry was dimensioned accordingly, which can be seen in Fig. 4(c). Path planning is pivotal in manufacturing the test specimen. Almost all coupons used in the experiments described in this section involve only

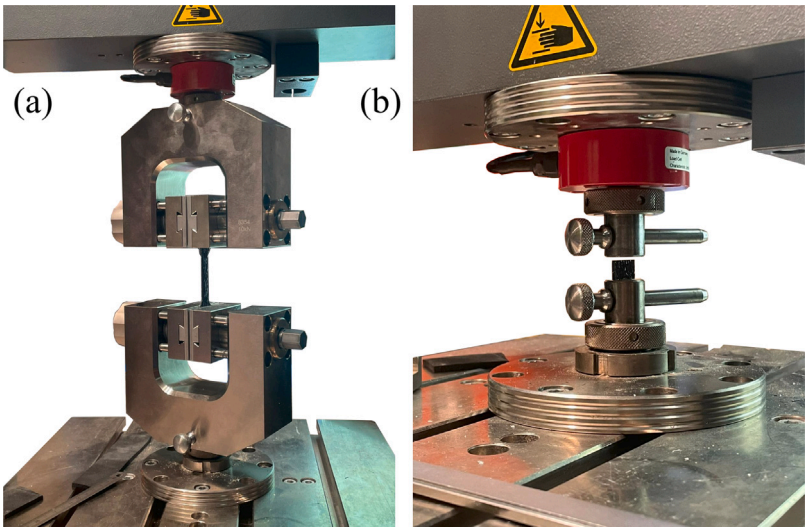

Fig. 5. Test setup on the ZwickRoell Z010 universal testing machine for the investigation of the effect of layer height variation on strength and Young's modulus. Tensile tests with dogbone geometry in (a) and compressive tests in (b).

zig-zag movements, where the only parameters for path planning are the geometry, layer height and path spacing. The X-dogbone where fiber direction aligns with the loading direction is the most difficult specimen to plan a path for, as the narrowing in the gauge section leads to isolated areas in the grip section that were connected into a single stroke using the approach described in [10]. This leads to the asymmetric path, which is not expected to have an impact on the strength of the part as the asymmetry only occurs in the thicker section of the dogbone. The paths for X- and Y-direction can be seen in Fig. 4(d) and (e) respectively.

As stated above, the dogbone geometry was chosen to be directly printed, requiring the direction changes during the zig-zag which can lead to twisted fiber bundles and thus negatively impact the surface quality. A hypothesis is, that for increasing layer height, these twisted fibers are not pressed against the deposited material as tightly as for lower layer height. As this nozzle pressure could mitigate the effects of twisted fibers on the surface quality, the surface quality could be expected to decrease with increasing layer height. To evaluate the impact on surface quality of layer height, especially focused on direction changes without cuts aligning with the point of direction change, white light interferometric (WLI) measurements of a critical region are performed.

The compressive tests are designed according to the tests for strength of the EN ISO 604 as cuboids with side lengths 10×10×4mm. The coupons are cut from a test plate measuring 40×34xH mm, with H corresponding to the lowest total height exceeding 4 mm for each layer height. To test the influence of fiber orientation and FVF, 3 specimens are tested for every fiber orientation X, Y with $h \in [0.4, 0.5, 0.6, 0.7]$ resulting in 24 specimens over all and $H \in [4, 4, 4.2, 4.2]$. The reasoning for choosing only 3 specimens to be tested instead of 6 is the smaller expected deviation as the samples were cut from one block with high precision and not directly printed, which is more prone to higher geometrical variance. The ability to cut them from one block also motivated the choice to test 4 layer heights instead of 3 as the additional required time is less in this method. Cutting was done on a ATM brilliant 220 precision wet abrasive cutting machine with water cooling and a corundum blade to avoid the thermoplastic melting and affecting the results. The same universal testing machine is used as in the tensile tests, the configuration with the compressive specimen can be seen in Fig. 5(b).

3. Results

This section aims at describing the results found in the experiments described above. Starting with the layer height, a selection of printed test coupons can be seen in the top row of Fig. 6. Successful print results could only be obtained for layer heights of 0.3 mm and above. For a layer height of 0.2 mm, no specimen could be manufactured due to failed prints. For some 0.25 mm specimen, successful printing could be achieved after several attempts, but the results showed mangled fibers and fiber breakage. The printing system clogged in almost all attempts for these layer heights, for all other layer heights the printing process was successful.

In order to further examine the layer height range for which printing is recommended and find the optimal upper and lower bound for load oriented printing, the layer height range $[0.3, 0.35, 0.4, 0.6.0.7, 0.8]$ in millimeters was chosen. The first three values represent possible minimum layer heights, and the last three represent their respective doubled value as maximum layer heights. This is done as $2h_{min} \leq h_{max}$ has to be followed for the slicing process. For this layer height range, coupons with a cross-section of 10×5 mm were printed and embedded in resin, ground and polished. The results of the micrographs are examined under a Keyence VHX-X1F optical microscope and can be seen in Fig. 7.

As can be expected, the micrographs show the amount of fiber in each coupon and thus the FVF decreasing with increasing layer height. The position of the fibers can be identified to be orderly, seen in the orthogonal mesostructure pattern of fiber and co-matrix. Upon closer inspection, though, the fiber placement can be seen to deviate from its expected position in the orthogonal grid. In the micrographs the coupons are oriented as they were printed with the print bed at the bottom of the respective image. This allows the observation that the fiber position is generally located at the top side of the deposited bead for all layer heights. Further examining the CFC material's cross-section shape, for 0.3 mm it is flattened for all beads into an elliptical shape. This effect is present in single instances for 0.35 mm and 0.4 mm, but not for higher layer heights. Pores and voids in the microstructure of the CCF material are especially present at 0.3 mm, where almost all CCF strands exhibit a high amount of voids up to the point where the strand is completely mangled, as can be seen in Fig. 8. For increasing layer height, this becomes less prominent, with the samples above 0.4 mm exhibiting almost no signs of this effect.

Furthermore, for layer height starting at 0.6 mm, diamond shaped gaps typical for FFF can be seen. These gaps are increasingly prominent for larger layer heights. Macrostructurally it can additionally be

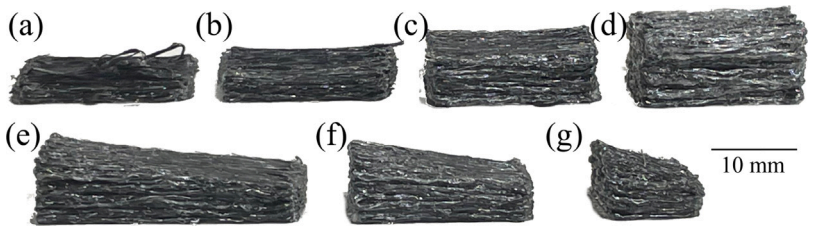

Fig. 6. Printed test coupons for determining the minimum and maximum possible layer heights for (a): 0.25 mm, (b): 0.3 mm, (c): 0.6 mm and (d): 0.9 mm layer height and dynamic layer height variation for (e): 30 mm, (f): 20 mm and (g): 10 mm length. All coupons could be printed successfully except for the 0.25 mm specimen.

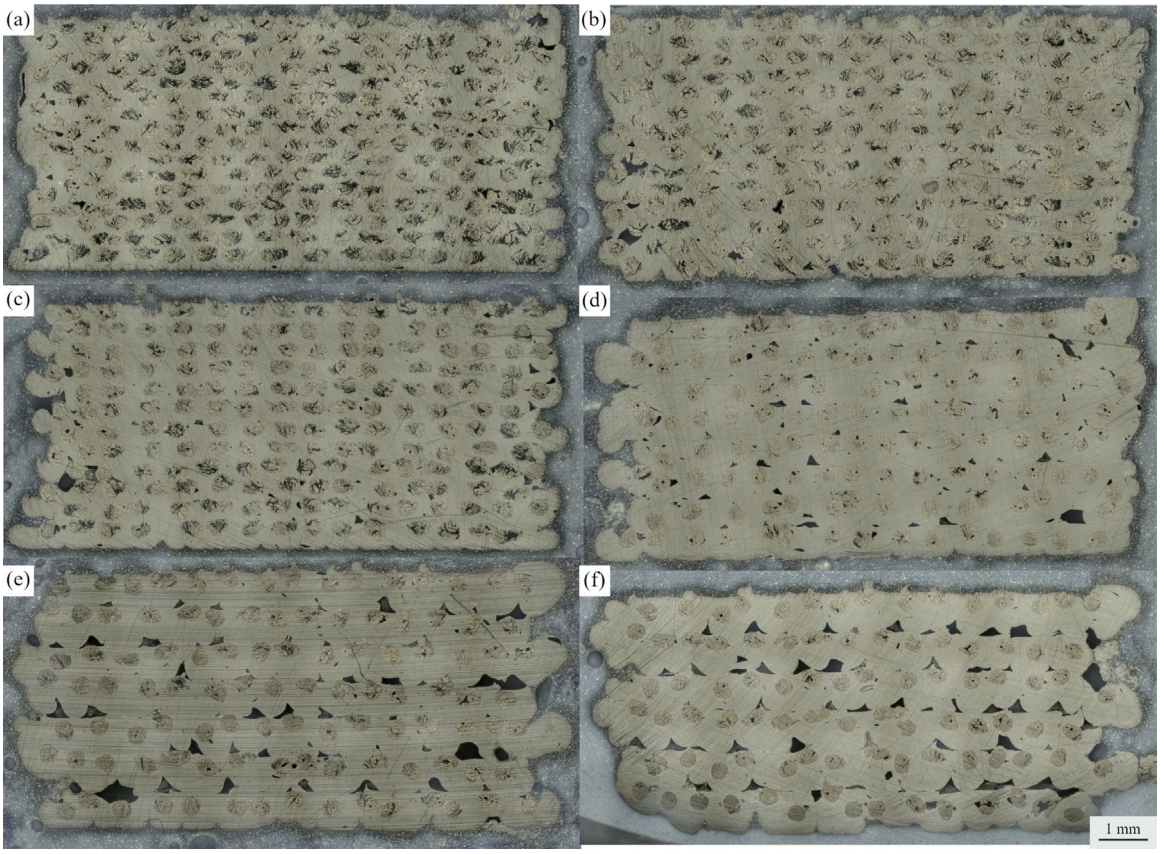

Fig. 7. Micrographs of printed, cut, ground and polished coupons with a cross-section of 10 × 5 mm to investigate the presence of cracks, voids, fiber bundle position and shape. Tested layer heights (a) 0.3 mm, (b) 0.35 mm, (c) 0.4 mm, (d) 0.6 mm, (e) 0.7 mm, (f) 0.8 mm.

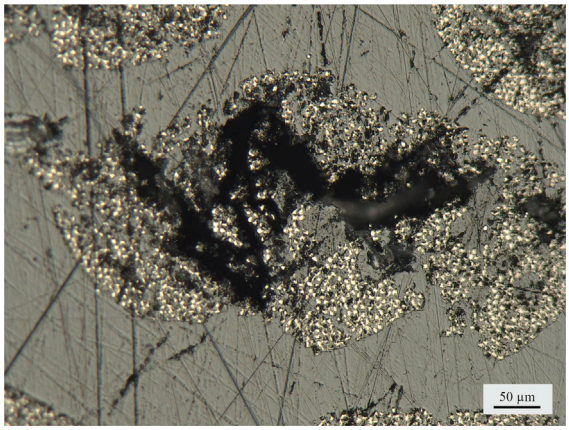

Fig. 8. Mangled and cracked deposited bead cross-section from the micrographs with 0.3 mm layer height.

observed, that the side walls of the samples have larger deviation from the rectangular target cross-section for higher layer heights.

For samples cut from the same block that the micrographs were done with, the fiber content as mass fraction is determined adhering to the DIN EN 2564 by extraction of the resin by sulfuric acid digestion. The results can be seen in Fig. 9. As expected, the fiber mass fraction follows an almost linear trend for increasing layer height.

For all tests of dynamic layer height variation, shown in Fig. 6(e)–(g), the deposition was successful and error free. The minimum layer height was chosen to be 0.3 mm and the maximum 0.7 mm. The same successful deposition was the case for the two parts printed to verify the process applicability, which can be seen in Fig. 10. For the tube-part, α was set to 1.5 as it was printed as a single wall, where no neighboring material exist to support the bead. For the bracket-part, the support material was printed first upon which the fiber material was placed, with no visible material on the part remaining after removal. For correct deposition, the positional calibration of the two print head base coordinate systems was essential to ensure correct alignment.

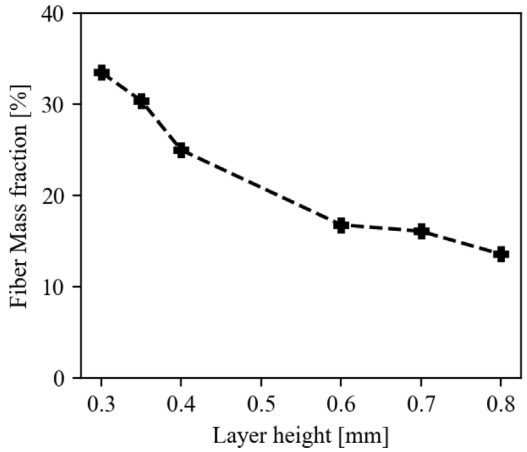

Fig. 9. Fiber mass fractions in percentage graphed over tested layer heights.

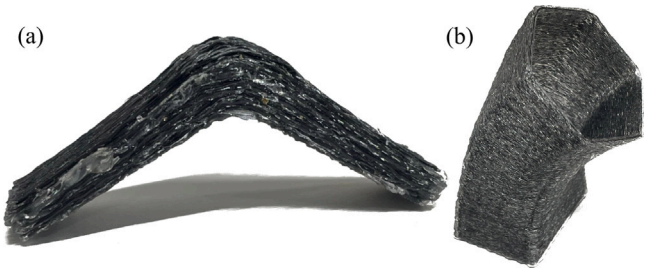

Fig. 10. Results for printed tests parts to evaluate applicability of the process with layer height variation. (a) V-Bracket with dimensions 10 mm x 43.5 mm x 17.3 mm and (b) Tube structure to demonstrate the variation of layer thickness and reduction of necessary layers and non-planar deposition with dimensions 42 mm x 52.5 mm x 76.7 mm.

During printing of the mechanical tests, some process stability issues arose. The X-specimens, which have the load direction aligned with the fibers, could all successfully be printed. Some of the Y-specimens, especially for the lower layer heights, exhibited problems in the neck area of the dogbone geometry. This is the section where many zig-zag movements are necessary. The problems were identified to be due to fiber being pulled with the nozzle after a direction change, which lead to the continuing fiber feed clogging the nozzle.

In Fig. 11 the results of the mechanical test can be seen. The top row shows the strengths for all mechanical experiments, the middle two rows show the stress–strain curves for the tensile tests, and the bottom two rows show the curves for the compressive tests. To obtain strain from the displacements, the displacements were divided by the length of the tested geometry. For the tensile specimen, this was set as 30 mm, corresponding to the neck area of the dogbone. For the compressive specimen, the total length of 10 mm was used. To compute the stress, the force was divided by the cross-section area of each specimen, which varied for the tensile tests in X and Y direction. This is due to the specimen's thickness being dictated by the layer height, as three layers each were printed such that the area is $10.4 * H$.

Firstly, the composite material's high degree of anisotropy can be confirmed by comparing the X specimen's strength where the fibers align with the load and the Y specimens where the load is orthogonal to the fiber direction. For this comparison the mean strengths are noted in Table 2, from which the degree of anisotropy is computed as the fraction of the X and Y specimen. The anisotropy can be observed to be the highest for the tensile specimen with lowest layer height. When looking at the individual layer heights it can be identified as decreasing with fiber volume fraction for all tests. The test results show a clear stepwise decrease in strength with decreasing fiber volume fraction for the X-tests. For the Y-tests, the strength is shown to be almost constant over layer heights. The high difference in strength regarding fiber orientation again shows the anisotropy of the material. The failure mode for the tensile tests was ripping of the fibers with fiber pullout for the X-tests and co-matrix breakage for the Y-tests. No delamination was observed. For the compressive tests the failure mode was crushing and fiber microbuckling also called kinking, no delamination or buckling was observed either.

The stress–strain curves of all tests show consistent results, except for two outliers for the tensile Y-tests with 0.3 mm layer height and a single outlier for the compressive X-tests with 0.7 mm layer height. In order to compute the Young's modulus, the curves were used to identify $x = \epsilon_{max}/4$ as the point to compute stiffness with ϵ_{max} corresponding to the strain at the maximum observed stress. The point was chosen, as all curves show almost linear behavior in this range. The linear approximation curves resulting from the mean of all computed Young's moduli of a test can be seen as dotted red lines in the curves in Fig. 11. The Young's moduli are plotted in Fig. 12. These results show the stiffness decreasing with increasing layer height and thus decreasing FVF for the X-tests. This effect is more pronounced for the tensile specimen and for the compressive specimen even a small increase can be seen for the small layer heights. The Y-tests show no significant variation over layer height.

In order to test the surface quality in critical regions where direction changes are done without a cut aligning with the point of direction change, a white light interferometer was used to obtain point clouds of the surface. The results of this investigation can be seen in Fig. 13. The Figure shows the inspected area of the part on the left, the point clouds from the WLI are shown in the top row and the histograms of the z-values are shown in the bottom row. The point clouds are precomputed with statistical outlier removal. Looking at the top row of point clouds, where the z-values are indicated by color, the twisted fibers can be identified, but no visible feature differences in the specimen can be made out. The histograms shown in the bottom row paint a similar picture, where the plots do not show clear differences in shape, except for a slightly wider distribution at 0.3 mm layer height. The standard deviation is shown in green dotted lines and for the histograms the following roughness values are computed: R_a is the arithmetic mean roughness, R_q is the root-mean-square roughness and R_z maximum height of the profile. All of these roughness measures do not show an increase of surface roughness for increasing layer heights. R_z even shows a decrease for higher layer heights.

4. Discussion

The results presented in the previous section are discussed and interpreted in this section.

The reason for the prints with a layer height below 0.3 mm failing is believed to be insufficient space for the CCF material under the nozzle. This leads to the fiber being crushed, as its diameter of 0.35 mm is significantly larger than these lower layer heights. The deformation or crushing effect can also be seen in the micrographs. Even if the deposition could successfully be realized, it is believed that too little co-matrix would prevent the formation of a functional composite. The observed clogging of the print head is attributed to the CCF material being pulled with the nozzle in points of direction changes, and also due to missing space under the nozzle. This leads to the opposing force on the fiber feed exceeding a limit where the fiber can still be pushed into the already deposited material, after which the CCF material buckles and accumulates above the hotend.

Regarding the micrographs, the varying fiber position in the mesostructure is believed to be caused by slightly wavy deposition. This is highly dependent on the CCF material's movement under the nozzle and could have several causes, which is why it should be examined in simulation and experimentally investigated in future works. An immediate assumption to solve this issue would be to decrease fiber

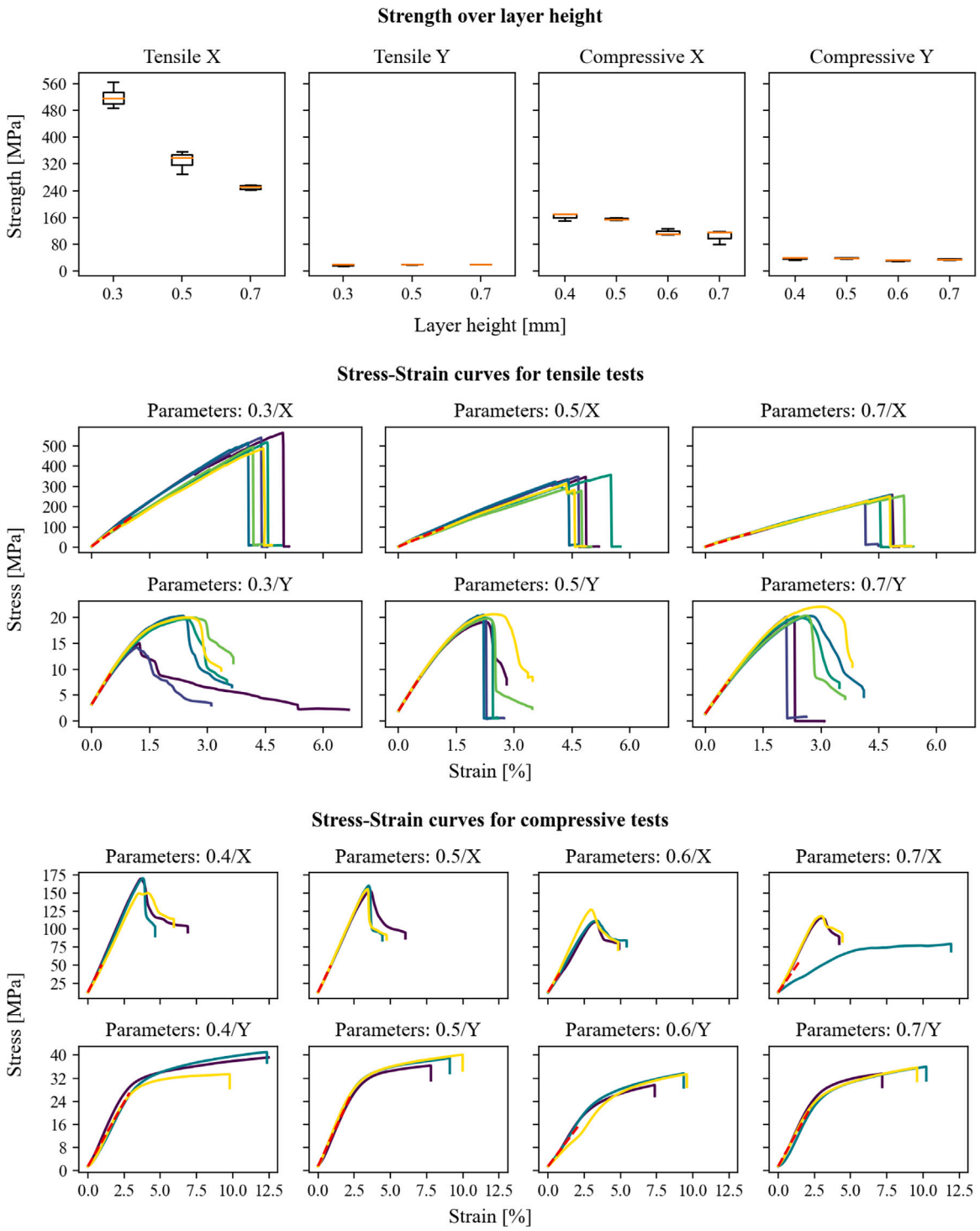

Fig. 11. Results for the experimental investigations on mechanical properties. X denotes the tests where the load aligns with the fibers and Y where the load is orthogonal to the fiber direction. The top row shows the strength over the tested layer heights and fiber orientations for the tensile and compressive tests. The middle two rows show the stress–strain curves for the tensile tests, and the bottom two rows show the curves for the compressive tests. The dotted red lines indicate the linear approximation curves resulting from the mean of all computed Young's moduli. (For interpretation of the references to color in this figure legend, the reader is referred to the web version of this article.)

feed rate, but the CCF material is believed to already be fully taut during deposition, shown by the fiber position at the top side of the bead in the micrographs. Furthermore, the robots accuracy of 0.02 mm can also not be excluded as an influencing factor on the fibers positional deviations. The use of a more accurate machine is desirable to eliminate this factor in the future. The elliptical shape of the CCF material caused by deformation and the tight bending at the orifice for the lower layer heights could also have an impact on the performance of the material. Hu et al. and Parker et al. found that the printing process itself can negatively impact the strength of the material by up to 60% [52,53]. A similar effect is expected to be caused by the voids inside the filament that are resulting from this deformation during printing. A possible strategy to decrease these voids could be to increase printing temperature or a different nozzle geometry. If they are created inside

Table 2
Mean strengths observed in the experiments and computed degree of anisotropy.

Specimen	Mean Strength X [MPa]	Mean Strength Y [MPa]	Anisotropy as X/Y
Tensile/0.3 mm	519.57	18.24	28.49
Tensile/0.5 mm	330.94	20.02	16.53
Tensile/0.7 mm	247.19	20.54	12.03
Compr./0.4 mm	163.17	38.22	4.27
Compr./0.5 mm	155.92	38.47	4.05
Compr./0.6 mm	116.12	32.22	3.6
Compr./0.7 mm	104.36	35.05	3

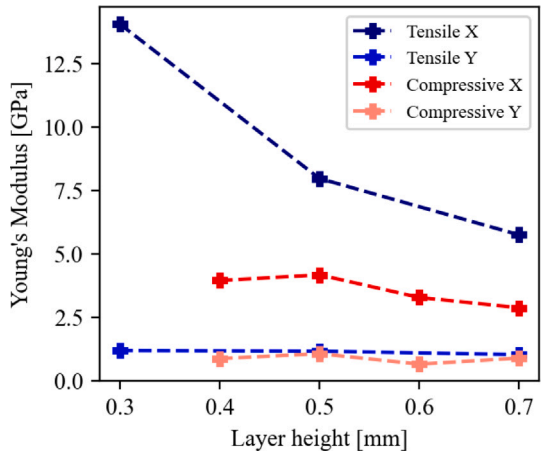

Fig. 12. Young's moduli computed from the stress–strain curves in Fig. 11 plotted over the tested layer heights.

the hotend, possible different mixing chamber designs might constitute a solution. The gaps seen in the micrographs for the higher layer heights are believed to be caused by undefined extrusion geometry above the path width of 0.65 mm. A solution to this problem could be increasing the path spacing, but this would severely decrease fiber volume fraction. The deciding factor in this choice would be if lower FVF or the gaps have higher impact on the mechanical performance. This should be the object of further study, explicitly including shear tests, as gaps are believed to have a higher impact on shear strength. Regarding the macrostructure, the coupons sidewalls were shown to exhibit wavy features. The geometrical accuracy of printed parts could be analyzed in the future.

The evaluation of fiber mass fraction showed the expected linearly decreasing trend with increasing layer height. A thing to note is the difference to FVF. The measurement was done by gravimetry, resulting in no voids being included in the measurement. This leads to slightly higher results compared to the expected results for FVF. However, both the observed results for fiber mass fraction and the slightly lower expected results for FVF are still in a competitive range for printed CFRP parts.

The successful deposition of the dynamic test coupons shows the capability of the system to achieve the layer height range dynamically. The printed parts do not represent the full spectrum of manufacturable parts in any way but verify the applicability to real world parts. Further application of the process to parts that are functionally validated or printed load optimally should be done. The ability to remove the support material also verifies the process of using this support material to print non-planar parts.

The stability issues observed during printing of the tensile test specimens can be attributed to the frequent direction changes without the cut aligning with the points of direction change. This phenomenon should be investigated further, especially the effect of cooling and compaction or path movements like hammering in order to avoid the fiber being pulled with the nozzle. Another measure would be the reduction of direction changes as much as possible by reducing the minimum cut distance of the print head, which would enable more geometries to be printed with the cuts aligning with the direction changes.

In the tests to evaluate the influence of layer height on the stiffness and strength of CFRP, there were two curves with high deviation for tensile Y with 0.3 mm layer height and one curve with high deviation for the compressive X tests with 0.7 mm layer height. As 6 specimens each were tested for the tensile and 3 for the compressive, these could be identified as outliers. The variance on the strength data is sufficiently small to allow conclusive evaluation.

As no extensometer was used in the experiments, the calculation of strain for the tensile tests is inaccurate. The usage of the neck length introduces errors in the calculation. As the claims of this paper are merely to analyze the effect of layer height variation, this is accepted and the focus of the evaluation is put on the trends over layer height and not on the absolute values. The CCF material's anisotropy is clearly confirmed by the difference in X and Y directions. The decreasing anisotropy with decreasing FVF seen in Table 2 align with the expectation, as only the CCF material exhibits anisotropic properties and the co-matrix is expected to behave isotropically. This can also explain the constant strength over layer height for the Y-tests and thus underline the effect of FVF on anisotropy. The same analysis can be transferred to the Young's moduli. Due to the presence of less anisotropic fibers, the Young's moduli decrease with decreasing FVF, but only for the X-tests with the tensile tests being the most prominent. The failure mode of crushing for the compressive specimens instead of buckling is attributed to the coupon geometry, which has a high area moment of inertia for a short length. All in all, it can be said that the observed behavior is as expected. This leads to the conclusion that the most prominent effect of layer height is the variation of FVF, which should be integrated into the design and analysis of parts and components.

The experiments done in this work inform the reasoning that 0.3 mm should be chosen as a minimum layer height and 0.6 mm should be chosen as a maximum layer height, with the possibility to extend this to 0.65 mm for some headroom in the slicing algorithms.

The roughness measures showed no significant effect on surface quality in points of direction change. The hypothesis of decreased surface roughness for lower layer heights due to the nozzle pressing the twisted fibers flat could not be verified. The slightly wider distribution seen for the lowest layer height of 0.3 mm could even indicate higher surface roughness due to fiber twisting and crushing. This effect of increased surface roughness was hypothesized by Parker et al. to be due to the flexure forces that develop for smaller layer heights [54]. Fiber crushing due to the printing process itself was furthermore identified to have a high negative impact on the printed parts strength [52,53]. If these surface imperfections are to be avoided, the conclusion could be to try to align the cuts to the point of direction change, which would eliminate the twisting of fibers.

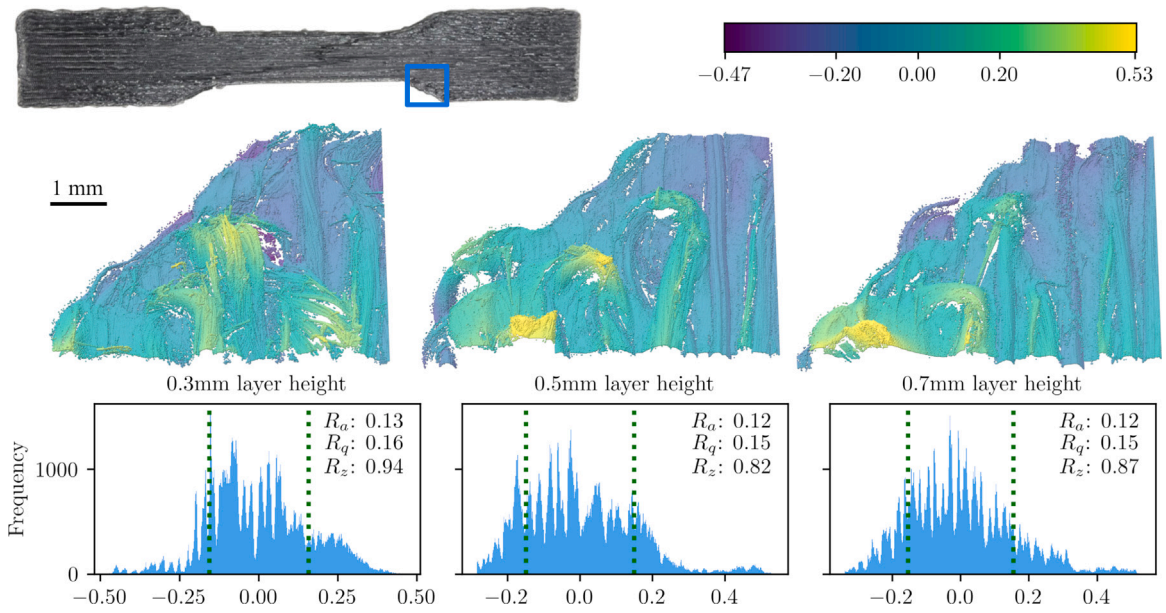

Fig. 13. Surface quality evaluation regarding roughness using white light interferometry. The most severe surface imperfection can be observed at points of direction change, seen in the blue square for a tensile test specimen. The marked area was scanned with the resulting point clouds plotted in the top row for 0.3 mm, 0.5 mm and 0.7 mm respectively. The bottom row shows the histograms of z-values in millimeters for the different layer heights. The green dotted line indicates the standard deviation. (For interpretation of the references to color in this figure legend, the reader is referred to the web version of this article.)

5. Conclusion and outlook

In this work, the possibility of dynamically varying layer height in order to enable load oriented non-planar printing of CFRP parts is investigated. With the experiments and their evaluation, the research questions established in Section 1.1 can be answered as follows:

1. Continuous fiber coextrusion can be applied to non-planar multi-axis printing by controlling the relative ratio of co-matrix material feed. Additionally, a printing head with a cutting unit and high clearance angle and a collision avoiding printing system with the dedicated extrusion control derived in this work enable the printing process.
2. An appropriate minimum layer height was shown to be 0.3 mm, with the maximum chosen as 0.65 mm to ensure the requirement of $2h_{min} \leq h_{max}$.
3. Layer height variation can be achieved dynamically.
4. The presented process and method can be used to manufacture parts.
5. Strength decreases for increasing layer height and thus decreasing fiber volume fraction. The composite's anisotropy could be confirmed, while stiffness was also shown to decrease with increasing layer height. No further negative effects of layer height variation were observed.
6. Quality regarding voids was analyzed and evaluated depending on layer height. Lower layer heights tend to introduce voids and cracks into the CCF material, higher layer heights can cause diamond shaped gaps between the deposited beads. While voids could be identified, no significant negative impact of layer height variation in the proposed range could be observed.

To answer these questions, the process is described, a dedicated extrusion control scheme is derived, and an experimental plan is proposed and explained. The layer height range was tested by manufacturing coupons. An appropriate range was then printed, cut, ground, polished and inspected under a microscope to identify fiber distribution, bead position and voids. Furthermore, fiber mass fraction was determined experimentally. The dynamic layer height variation and manufacturability of parts could be confirmed through dedicated experiments. Mechanical tests were done to evaluate the influence of layer height variation on the strength and stiffness. Surface quality was evaluated using white light interferometry.

Future work should include the printing and evaluation of more complex parts which use non-planar multi-axis printing with layer height variation. This would enable and should include a more general evaluation of the effect of non-planar printing on stiffness and strength of parts manufactured using the method at the center of this work. The effects of the process parameters on void content and stiffness and strength could further be examined. During these tests, the void content and general porosity should be compared to classical FFF and towpreg extrusion in quantitative and qualitative form. In addition to varying layer height, the extrusion width could be varied dynamically in order to avoid gaps between the paths. This could be a promising next step to decrease gaps between the paths in more complex parts. Printing reliability could be increased by looking into core problems of the process. The main challenge is nozzle clogging at direction changes where the cut does not align with the point of direction change. The nozzle pulling the fiber with it and hysteresis under the nozzle lead to incorrect deposition. An option for solving this problem could be specialized compaction movements like hammering at these points or introducing part cooling to speed up the co-matrix solidification process. Part cooling would require a specialized cooling solution with a high clearance angle in order to avoid collisions in the multi-axis printing process. Cutting could be employed to prevent fiber wrinkling, buckling, or splitting in the turning points. These effects could be further investigated using profilometry. To employ cutting as a solution requires a shorter minimum fiber cut length for shorter paths. Lastly, the process stability and incorrect or wavy deposition should be analyzed in a simulation and experimentally investigated.

CRediT authorship contribution statement

Johann Kipping: Writing – original draft, Visualization, Validation, Software, Methodology, Investigation, Formal analysis, Data curation, Conceptualization. **Thorsten Schüppstuhl:** Writing – review & editing, Supervision, Resources, Project administration.

Acknowledgment

All authors have read and agreed to the published version of the manuscript.

Funding:

This work was supported by the Deutsche Forschungsgemeinschaft (DFG, German Research Foundation), Germany — Grant number 550194375

Declaration of competing interest

The authors declare that they have no known competing financial interests or personal relationships that could have appeared to influence the work reported in this paper.

Data availability

All of the data acquired in the experimental evaluation is provided in paper or upon inquiring with the author.

References

[1] Yuan Yang, Bo Yang, Zhengping Chang, Jihao Duan, Weihua Chen, Research status of and prospects for 3D printing for continuous fiber-reinforced thermoplastic composites, Polymers (ISSN: 2073-4360) 15 (17) (2023) http://dx.doi.org/10.3390/polym15173653.

[2] Ping Cheng, Yong Peng, Shixian Li, Yanni Rao, Antoine Le Duigou, Kui Wang, Said Ahzi, 3D printed continuous fiber reinforced composite lightweight structures: A review and outlook, Compos. Part B: Eng. (ISSN: 1359-8368) 250 (2023) 110450, http://dx.doi.org/10.1016/j.compositesb.2022.110450, URL https://www.sciencedirect.com/science/article/pii/S135983682200823X.

[3] Denizhan Yavas, Ziyang Zhang, Qingyang Liu, Dazhong Wu, Fracture behavior of 3D printed carbon fiber-reinforced polymer composites, Compos. Sci. Technol. (ISSN: 0266-3538) 208 (2021) 108741, http://dx.doi.org/10.1016/j.compscitech.2021.108741, URL https://www.sciencedirect.com/science/article/pii/S026635382100097X.

[4] Ziyang Zhang, Denizhan Yavas, Qingyang Liu, Dazhong Wu, Effect of build orientation and raster pattern on the fracture behavior of carbon fiber reinforced polymer composites fabricated by additive manufacturing, Addit. Manuf. (ISSN: 2214-8604) 47 (2021) 102204, http://dx.doi.org/10.1016/j.addma.2021.102204, URL https://www.sciencedirect.com/science/article/pii/S2214860421003651.

[5] Hung Le, Denizhan Yavas, Dazhong Wu, Flexural and fracture behavior of additively manufactured carbon fiber reinforced polymer composites with bioinspired bouligand meso-structures, Compos. Struct. (ISSN: 0263-8223) 323 (2023) 117436, http://dx.doi.org/10.1016/j.compstruct.2023.117436, URL https://www.sciencedirect.com/science/article/pii/S0263822323007821.

[6] Qing Wang, Qing Zhang, Yuzhu Kang, Yesong Wang, Jiang Liu, An investigation of preparation of continuous carbon fiber reinforced PLA prepreg filament, Compos. Commun. (ISSN: 2452-2139) 39 (2023) 101530, http://dx.doi.org/10.1016/j.coco.2023.101530, URL https://www.sciencedirect.com/science/article/pii/S2452213923000384.

[7] Ben Wang, Yueke Ming, Ashraf Aboelenien, Gerhard Ziegmann, Feng Wang, Zhibo Xin, Xiao Hong, Jin Zhou, Yatao Zhao, Zhongqiu Ding, Yugang Duan, Improved structural efficiency in composite manufacturing via hammered printing for large-curvature fiber paths, Addit. Manuf. (ISSN: 2214-8604) 79 (2024) 103918, http://dx.doi.org/10.1016/j.addma.2023.103918, URL https://www.sciencedirect.com/science/article/pii/S2214860423005316.

[8] Kai Steltner, Johann Kipping, Thorsten Schüppstuhl, Benedikt Kriegesmann, A workflow for designing stiffness-optimized structures in the context of additive manufacturing of endless fiber-reinforced composites, J. Thermoplast. Compos. Mater. 08927057251332788, http://dx.doi.org/10.1177/08927057251332788.

[9] Guoxin Fang, Tianyu Zhang, Sikai Zhong, Xiangjia Chen, Zichun Zhong, Charlie C.L. Wang, Reinforced FDM: Multi-axis filament alignment with controlled anisotropic strength, ACM Trans. Graph. (ISSN: 0730-0301) 39 (6) (2020) http://dx.doi.org/10.1145/3414685.3417834.

[10] Johann Kipping, Doran Nettig, Thorsten Schüppstuhl, Looping: Load-oriented optimized paths in non-planar geometry, Addit. Manuf. (ISSN: 2214-8604) (2024) 104426, http://dx.doi.org/10.1016/j.addma.2024.104426, URL https://www.sciencedirect.com/science/article/pii/S221486042400472X.

[11] Johann Kipping, Thorsten Schüppstuhl, Load-oriented nonplanar additive manufacturing method for optimized continuous carbon fiber parts, Materials (ISSN: 1996-1944) 16 (3) (2023) http://dx.doi.org/10.3390/ma16030998, URL https://www.mdpi.com/1996-1944/16/3/998.

[12] Guoxin Fang, Tianyu Zhang, Yuming Huang, Zhizhou Zhang, Kunal Masania, Charlie C.L. Wang, Exceptional mechanical performance by spatial printing with continuous fiber: Curved slicing, toolpath generation and physical verification, Addit. Manuf. (ISSN: 2214-8604) 82 (2024) 104048, http://dx.doi.org/10.1016/j.addma.2024.104048, URL https://www.sciencedirect.com/science/article/pii/S2214860424000940.

[13] Tianyu Zhang, Tao Liu, Neelotpal Dutta, Yongxue Chen, Renbo Su, Zhizhou Zhang, Weiming Wang, Charlie C.L. Wang, Toolpath generation for high density spatial fiber printing guided by principal stresses, Compos. Part B: Eng. (ISSN: 1359-8368) 295 (2025) 112154, http://dx.doi.org/10.1016/j.compositesb.2025.112154, URL https://www.sciencedirect.com/science/article/pii/S1359836825000447.

[14] Denizhan Yavas, Ziyang Zhang, Qingyang Liu, Dazhong Wu, Interlaminar shear behavior of continuous and short carbon fiber reinforced polymer composites fabricated by additive manufacturing, Compos. Part B: Eng. (ISSN: 1359-8368) 204 (2021) 108460, http://dx.doi.org/10.1016/j.compositesb.2020.108460, URL https://www.sciencedirect.com/science/article/pii/S1359836820335095.

[15] Narongkorn Krajangsawasdi, Lourens G. Blok, Ian Hamerton, Marco L. Longana, Benjamin K.S. Woods, Dmitry S. Ivanov, Fused deposition modelling of fibre reinforced polymer composites: A parametric review, J. Compos. Sci. (ISSN: 2504-477X) 5 (1) (2021) http://dx.doi.org/10.3390/jcs5010029.

[16] Chrysoula Pandelidi, Stuart Bateman, Sebastian Piegert, Rene Hoehner, Ingomar Kelbassa, Milan Brandt, The technology of continuous fibre-reinforced polymers: a review on extrusion additive manufacturing methods, Int. J. Adv. Manuf. Technol. (ISSN: 1433-3015) 113 (11) (2021) 3057–3077, http://dx.doi.org/10.1007/s00170-021-06837-6.

[17] Adi Adumitroaie, Fedor Antonov, Aleksey Khaziev, Andrey Azarov, Mikhail Golubev, Valery V. Vasiliev, Novel continuous fiber bi-matrix composite 3-D printing technology, Materials (ISSN: 1996-1944) 12 (18) (2019) http://dx.doi.org/10.3390/ma12183011.

[18] Andrey Valerievich Azarov, Fedor Konstantinovich Antonov, Mikhail Valerievich Golubev, Aleksey Ravkatovich Khaziev, Production of articles made of composite materials by 3D-printing method, (US11673322B2) 2017.

[19] A.V. Azarov, V.A. Kolesnikov, A.R. Khaziev, Development of equipment for composite 3D printing of structural elements for aerospace applications, IOP Conf. Ser.: Mater. Sci. Eng. (ISSN: 1757-8981) 934 (1) (2020) 012049, http://dx.doi.org/10.1088/1757-899X/934/1/012049.

[20] José Humberto S. Almeida, Siddharth Jayaprakash, Kari Kolari, Jukka Kuva, Kirsi Kukko, Jouni Partanen, The role of printing parameters on the short beam strength of 3D-printed continuous carbon fibre reinforced epoxy-PETG composites, Compos. Struct. (ISSN: 0263-8223) 337 (2024) 118034, http://dx.doi.org/10.1016/j.compstruct.2024.118034, URL https://www.sciencedirect.com/science/article/pii/S0263822324001624.

[21] Macrolayers Technology, , 2024, https://docs.aura3d.tech/aura/macrolayers/. (19 August Accessed: 2024).

[22] Marina Andreozzi, Serena Gentili, Pietro Forcellese, Tiziano Bellezze, Valeria Corinaldesi, Francesca Luzi, Alessio Vita, Effect of moisture content on the mechanical performance of 3D printed continuous reinforced two-matrix composite, Int. J. Adv. Manuf. Technol. (ISSN: 1433-3015) 133 (11) (2024) 5117–5126, http://dx.doi.org/10.1007/s00170-024-14041-5.

[23] Jingmin Gao, Binbin Li, Hengchang Bu, Xiaodong Li, Xiaohong Zhan, Effect of infill density and reinforced perimeters on tensile properties and fracture mechanism of 3D printing carbon fiber-reinforced composite, Int. J. Adv. Manuf. Technol. (ISSN: 1433-3015) 128 (1) (2023) 267–281, http://dx.doi.org/10.1007/s00170-023-11871-7.

[24] He Kong, Peng Qu, Xunjin Li, Dekun Kong, Anfu Guo, Shaoqing Wang, Yi Wan, Jun Takahashi, An investigation into mechanical properties of a 3D printed two-matrix continuous fiber composites with multi-cavity structure, J. Mater. Res. Technol. (ISSN: 2238-7854) 26 (2023) 4365–4386, http://dx.doi.org/10.1016/j.jmrt.2023.08.132, URL https://www.sciencedirect.com/science/article/pii/S2238785423019464.

[25] Fei Liu, Eleonora Ferraris, Jan Ivens, Mechanical investigation and microstructure performance of a two-matrix continuous carbon fibre composite fabricated by 3D printing, J. Manuf. Process. (ISSN: 1526-6125) 79 (2022) 383–393, http://dx.doi.org/10.1016/j.jmapro.2022.04.050, URL https://www.sciencedirect.com/science/article/pii/S1526612522002869.

[26] Alexander Matschinski, Dennis Bublitz, Thomas Ihring, Chih Yu Chen, Simon Grandl, Kilian Schneider, Garth Pearce, Klaus Drechsler, Optimization of continuous fiber path planning for an additively manufactured open-hole specimen, Mater. Sci. Forum (ISSN: 1662-9752) 1060 (2022) 127–132, http://dx.doi.org/10.4028/p-o3m3cd, URL https://www.scientific.net/MSF.1060.127.

[27] Chethan Savandaiah, Stefan Sieberer, Bernhard Plank, Julia Maurer, Georg Steinbichler, Janak Sapkota, Influence of rapid consolidation on co-extruded additively manufactured composites, Polymers (ISSN: 2073-4360) 14 (9) (2022) http://dx.doi.org/10.3390/polym14091838.

[28] Stefan Sieberer, Markus Winklberger, Chethan Savandaiah, Christoph Kralovec, Martin Schagerl, Experimental strength and fracture analysis of additively manufactured continuous carbon fibre reinforced lugs with load-tailored fibre placement, Procedia Struct. Integr. (ISSN: 2452-3216) 42 (2022) 72–79, http://dx.doi.org/10.1016/j.prostr.2022.12.008, URL https://www.sciencedirect.com/science/article/pii/S2452321622005650.

[29] Shouling Ding, Bin Zou, Pin Zhang, Qingyang Liu, Yuexi Zhuang, Zhiwei Feng, Fengchen Wang, Xinfeng Wang, Layer thickness and path width setting in 3D printing of pre-impregnated continuous carbon, glass fibers and their hybrid composites, Addit. Manuf. (ISSN: 2214-8604) 83 (2024) 104054, http://dx.doi.org/10.1016/j.addma.2024.104054, URL https://www.sciencedirect.com/science/article/pii/S2214860424001003.

[30] Hao Dou, Yunyong Cheng, Wenguang Ye, Dinghua Zhang, Junjie Li, Zhoujun Miao, Stephan Rudykh, Effect of process parameters on tensile mechanical properties of 3D printing continuous carbon fiber-reinforced PLA composites, Materials (ISSN: 1996-1944) 13 (17) (2020) http://dx.doi.org/10.3390/ma13173850.

[31] Samir Kasmi, Geoffrey Ginoux, Samir Allaoui, Sébastien Alix, Investigation of 3D printing strategy on the mechanical performance of coextruded continuous carbon fiber reinforced PETG, J Appl Polym Sci (ISSN: 0021-8995) 138 (37) (2021) 50955, http://dx.doi.org/10.1002/app.50955, URL https://doi.org/10.1002/app.50955.

[32] Bahri Barış Vatandaş, Altuğ Uşun, Recep Gümrük, Cemaleddin Şimşek, The relationship between fiber bundle size and mechanical performance of additively manufactured continuous carbon fiber reinforced thermoplastic composites, in: 3D Printing and Additive Manufacturing, 10 (6) (2023) 1190–1203, http://dx.doi.org/10.1089/3dp.2022.0220.

[33] Lijun Li, Wenyao Liu, Lingyu Sun, Mechanical characterization of 3D printed continuous carbon fiber reinforced thermoplastic composites, Compos. Sci. Technol. (ISSN: 0266-3538) 227 (2022) 109618, http://dx.doi.org/10.1016/j.compscitech.2022.109618, URL https://www.sciencedirect.com/science/article/pii/S0266353822003608.

[34] Fei Liu, Shenru Wang, Wuxiang Zhang, Xilun Ding, Eleonora Ferraris, Jan Ivens, Mechanical and interfacial analysis of 3D-printed two-matrix continuous carbon fibre composites for enhanced structural performance, Compos. Part A: Appl. Sci. Manuf. (ISSN: 1359-835X) 180 (2024) 108105, http://dx.doi.org/10.1016/j.compositesa.2024.108105, URL https://www.sciencedirect.com/science/article/pii/S1359835X24001027.

[35] Alberto Parmiggiani, Mirko Prato, Marco Pizzorni, Effect of the fiber orientation on the tensile and flexural behavior of continuous carbon fiber composites made via fused filament fabrication, Int. J. Adv. Manuf. Technol. (ISSN: 1433-3015) 114 (7) (2021) 2085–2101, http://dx.doi.org/10.1007/s00170-021-06997-5.

[36] Marius Rimašauskas, Elena Jasiūnienė, Tomas Kuncius, Rūta Rimašauskienė, Vaidotas Cicėnas, Investigation of influence of printing parameters on the quality of 3D printed composite structures, Compos. Struct. (ISSN: 0263-8223) 281 (2022) 115061, http://dx.doi.org/10.1016/j.compstruct.2021.115061, URL https://www.sciencedirect.com/science/article/pii/S0263822321014811.

[37] Denizhan Yavas, High-temperature fracture behavior of carbon fiber reinforced peek composites fabricated via fused filament fabrication, Compos. Part B: Eng. (ISSN: 1359-8368) 266 (2023) 110987, http://dx.doi.org/10.1016/j.compositesb.2023.110987, URL https://www.sciencedirect.com/science/article/pii/S1359836823004900.

[38] D. Yavas, Enhancing interlaminar shear strength in additively manufactured carbon fiber-reinforced thermoplastic composites through microstructural design, Exp. Mech. (ISSN: 1741-2765) 65 (4) (2025) 509–522, http://dx.doi.org/10.1007/s11340-025-01144-7.

[39] Javaid Butt, Raghunath Bhaskar, Vahaj Mohaghegh, Analysing the effects of layer heights and line widths on FFF-printed thermoplastics, Int. J. Adv. Manuf. Technol. (ISSN: 1433-3015) 121 (11) (2022) 7383–7411, http://dx.doi.org/10.1007/s00170-022-09810-z.

[40] Dirk Fischer, Claudia Eßbach, Robert Schönherr, Dagmar Dietrich, Daniela Nickel, Improving inner structure and properties of additive manufactured amorphous plastic parts: The effects of extrusion nozzle diameter and layer height, Addit. Manuf. (ISSN: 2214-8604) 51 (2022) 102596, http://dx.doi.org/10.1016/j.addma.2022.102596, URL https://www.sciencedirect.com/science/article/pii/S2214860422000045.

[41] S. Garzon-Hernandez, D. Garcia-Gonzalez, A. Jérusalem, A. Arias, Design of FDM 3D printed polymers: An experimental-modelling methodology for the prediction of mechanical properties, Mater. Des. (ISSN: 0264-1275) 188 (2020) 108414, http://dx.doi.org/10.1016/j.matdes.2019.108414, URL https://www.sciencedirect.com/science/article/pii/S0264127519308524.

[42] Lukas Pelzer, Christian Hopmann, Additive manufacturing of non-planar layers with variable layer height, Addit. Manuf. (ISSN: 2214-8604) 37 (2021) 101697, http://dx.doi.org/10.1016/j.addma.2020.101697, URL https://www.sciencedirect.com/science/article/pii/S2214860420310691.

[43] Naoya Kumekawa, Yuto Mori, Haruya Tanaka, Ryosuke Matsuzaki, Experimental evaluation of variable thickness 3D printing of continuous carbon fiber-reinforced composites, Compos. Struct. (ISSN: 0263-8223) 288 (2022) 115391, http://dx.doi.org/10.1016/j.compstruct.2022.115391, URL https://www.sciencedirect.com/science/article/pii/S026382232200191X.

[44] Peng Zhang, Shouzheng Sun, Jiaqi Duan, Hongya Fu, Zhenyu Han, Hongbo Geng, Yang Feng, Line width prediction and mechanical properties of 3D printed continuous fiber reinforced polypropylene composites, Addit. Manuf. (ISSN: 2214-8604) 61 (2023) 103372, http://dx.doi.org/10.1016/j.addma.2022.103372, URL https://www.sciencedirect.com/science/article/pii/S2214860422007618.

[45] Johann Kipping, Thore Kleibrink, Thorsten Schüppstuhl, Development of a print head for non-planar additive manufacturing of carbon fiber-reinforced polymers, Int. J. Adv. Manuf. Technol. (ISSN: 1433-3015) 139 (11) (2025) 5697–5714, http://dx.doi.org/10.1007/s00170-025-16079-5.

[46] Heng Cai, Yuan Chen, A review of print heads for fused filament fabrication of continuous carbon fiber-reinforced composites, Micromachines (ISSN: 2072-666X) 15 (4) (2024) http://dx.doi.org/10.3390/mi15040432.

[47] Andrey Valerievich Azarov, Mikhail Valerievich Golubev, Fedor Konstantinovich Antonov, Aleksey Ravkatovich Khaziev, Print head for additive manufacturing of articles, (US20200114578A1) 2017.

[48] Johann Kipping, Doran Nettig, Zsolt Kallai, Thorsten Schueppstuhl, A robotic printer for nonplanar additive manufacturing of carbon fiber reinforced polymers, in: ISR Europe 2023; 56th International Symposium on Robotics, 2023, pp. 205–212.

[49] Pinyi Wu, Keval S. Ramani, Chinedum E. Okwudire, Accurate linear and nonlinear model-based feedforward deposition control for material extrusion additive manufacturing, Addit. Manuf. (ISSN: 2214-8604) 48 (2021) 102389, http://dx.doi.org/10.1016/j.addma.2021.102389, URL https://www.sciencedirect.com/science/article/pii/S2214860421005431.

[50] Pinyi Wu, Chen Qian, Chinedum E. Okwudire, Modeling and feedforward control of filament advancement and retraction in material extrusion additive manufacturing, Addit. Manuf. (ISSN: 2214-8604) 78 (2023) 103850, http://dx.doi.org/10.1016/j.addma.2023.103850, URL https://www.sciencedirect.com/science/article/pii/S2214860423004633.

[51] Zsolt Kállai, Johann Kipping, Thorsten Schüppstuhl, Closing the Gap: Exploring Approaches for Printing Lightweight Curved Pipes with Carbon Fiber Reinforced Thermoplastics, vol. 8, The European Society for Composite Materials (ESCM) and the Ecole Centrale de Nantes, 2024, http://dx.doi.org/10.15480/882.13713, URL https://hdl.handle.net/11420/52078.

[52] Yiwei Hu, Raj B. Ladani, Milan Brandt, Yazhi Li, Adrian P. Mouritz, Carbon fibre damage during 3D printing of polymer matrix laminates using the FDM process, Mater. Des. (ISSN: 0264-1275) 205 (2021) 109679, http://dx.doi.org/10.1016/j.matdes.2021.109679, URL https://www.sciencedirect.com/science/article/pii/S0264127521002318.

[53] M. Parker, N. Ezeokeke, R. Matsuzaki, D. Arola, Strength and its variability in 3D printing of polymer composites with continuous fibers, Mater. Des. (ISSN: 0264-1275) 225 (2023) 111505, http://dx.doi.org/10.1016/j.matdes.2022.111505, URL https://www.sciencedirect.com/science/article/pii/S0264127522011285.

[54] M. Parker, A. Inthavong, E. Law, S. Waddell, N. Ezeokeke, R. Matsuzaki, D. Arola, 3D printing of continuous carbon fiber reinforced polyphenylene sulfide: Exploring printability and importance of fiber volume fraction, Addit. Manuf. (ISSN: 2214-8604) 54 (2022) 102763, http://dx.doi.org/10.1016/j.addma.2022.102763, URL https://www.sciencedirect.com/science/article/pii/S2214860422001671.